Eur Biophys J (1998) 27: 321–334

ARTICLE

Markus Blümel · Jürgen M. Schmidt · Frank Löhr
Heinz Rüterjans

Quantitative ϕ torsion angle analysis in *Desulfovibrio vulgaris* flavodoxin based on six ϕ related ^3J couplings

Received: 5 August 1997 / Accepted: 29 October 1997

Abstract Quantitative ϕ-dihedral angle determinations of non-glycine and non-proline residues in *Desulfovibrio vulgaris* flavodoxin are carried out on the exclusive basis of ^3J coupling constants. In total 124 $^3J_{H^NH\alpha}$, 123 $^3J_{H^NC'_i}$, 118 $^3J_{H^NC\beta}$, 117 $^3J_{C'_{i-1}H\alpha}$, 109 $^3J_{C'_{i-1}C'_i}$, and 103 $^3J_{C'_{i-1}H\beta}$ values form the experimental basis for translating J coupling data into geometry information using various combinations of Karplus parameters given in the literature. In addition, each backbone torsional angle ϕ is adjusted assuming different models of local geometry, either a rigid torsion, a Gaussian distribution centered at a distinct angle, or a two-site jump model. Numerical optimization is followed by a statistical significance evaluation to assess the results. It is found that experimental coupling constants of most of the residues involved in secondary structure elements agree best with those predicted from rigid local conformations. For dihedral angles in loop regions, mobility effects are not negligible, and a single torsion (Glu 42) is likely to adopt two distinct adjustments. However, α-helix conformations with $-60° < \phi < -45°$ give rise to an alternate solution with $\phi \approx +170°$ with similar statistical significance when using the four traditionally determined proton-involved ^3J couplings. This ambiguity is efficiently avoided only when taking advantage of the complete data set comprising six available experimental ^3J coupling constants and of the degeneracy intrinsic to the Karplus relation. The optimized ϕ conformations are compared with reference values from the crystal structure of flavodoxin.

Key words Vicinal coupling constants · Polypeptide ϕ angles · Karplus parameters · Least-squares optimization · Back-calculation of coupling constants

M. Blümel · J. M. Schmidt · F. Löhr · H. Rüterjans (✉)
Institut für Biophysikalische Chemie,
Johann Wolfgang Goethe-Universität Frankfurt,
Biozentrum N230, Marie-Curie-Strasse 9,
D-60439 Frankfurt/Main, Germany
e-mail: hruet@bpc.uni-frankfurt.de

Abbreviations *ANOVA* Analysis of variances · *COSY* Correlated spectroscopy · *E. COSY* Exclusive correlation spectroscopy · *FMN* Riboflavin 5′-monophosphate · *HMQC* Heteronuclear multiple-quantum coherence · *HSQC* Heteronuclear single-quantum coherence · *NMR* Nuclear magnetic resonance · *PFG* Pulsed field gradient · *TPPI* Time proportional phase incrementation

Introduction

Structure refinement of biological macromolecules on the basis of NMR spectroscopy (Roberts 1993) profits from angular constraints derived from accurately measured homo- and heteronuclear three-bond J coupling constants (Case et al. 1994; Biamonti et al. 1994; Eberstadt et al. 1995). Typically, loops located on the protein surface are imprecisely determined owing to the lack of NOE data or because of local dynamics effects. An independent analysis of vicinal coupling constants can provide additional information on both local geometry and angular mobility. The well-appreciated procedure to calculate ^3J coupling constants from a given molecular conformation was proposed by Karplus (1959, 1963) and is expressed by the following empirical relation

$$^3J(\theta) = A\cos^2\theta + B\cos\theta + C. \quad (1)$$

The dihedral angle θ is subtended by three consecutive covalent bonds that connect the pair of coupled nuclei, and A, B, and C are empirical coefficients given in Hertz which depend on the nature of the coupled nuclei as well as on their chemical environment.

This investigation focuses on the analysis of ^3J coupling constants related to the backbone torsion angle ϕ in proteins (Fig. 1). Owing to the intrinsic degeneracy in Eq. (1), the derivation of the dihedral-angle conformation from a single experimental ^3J coupling constant leads to up to four solutions (Fig. 2 a). In addition, motional averaging might affect the experimental coupling constants. In this case the ^3J values cannot be interpreted with a single rigid confor-

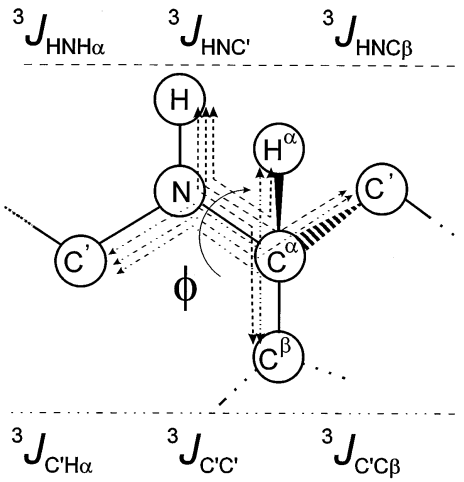

Fig. 1 Polypeptide-backbone fragment showing the torsion angle ϕ (C'_{i-1}-N-C^α-C'_i) and related *J* coupling interactions. *Arrows* indicate homo- and heteronuclear three-bond couplings examined in the context of the present investigation

mation (Jardetzky 1980; Hoch et al. 1985; Schmidt 1997). In a qualitative analysis, $^3J_{H^NH^\alpha}$ coupling constants are most easily exploited owing to their comparatively large magnitudes, where values below 5 Hz and above 8 Hz are usually diagnostic of α-helix and β-sheet conformations with ϕ dihedral angles in the vicinity of –60° and –120°, respectively. Intermediate coupling constants are usually ignored, critically assuming that rare conformations of the ϕ torsion as well as motional averaging are absent. Quantitative characterization of the ϕ torsion requires, firstly, the combined use of multiple coupling constants (Mierke and Kessler 1992), and secondly, considering angular motion as was demonstrated for peptides (Schmidt 1997). The success depends on the reliability of both the experimental coupling constants and the Karplus parameters used. Much effort, in theoretical as well as in experimental studies, has been devoted to the refinement of Karplus coefficients for the different types of coupled atom pairs relevant to amino-acid residues (Bystrov 1976; Wang and Bax 1996; Löhr et al. 1997). Karplus parameters are either derived from *ab-in-*

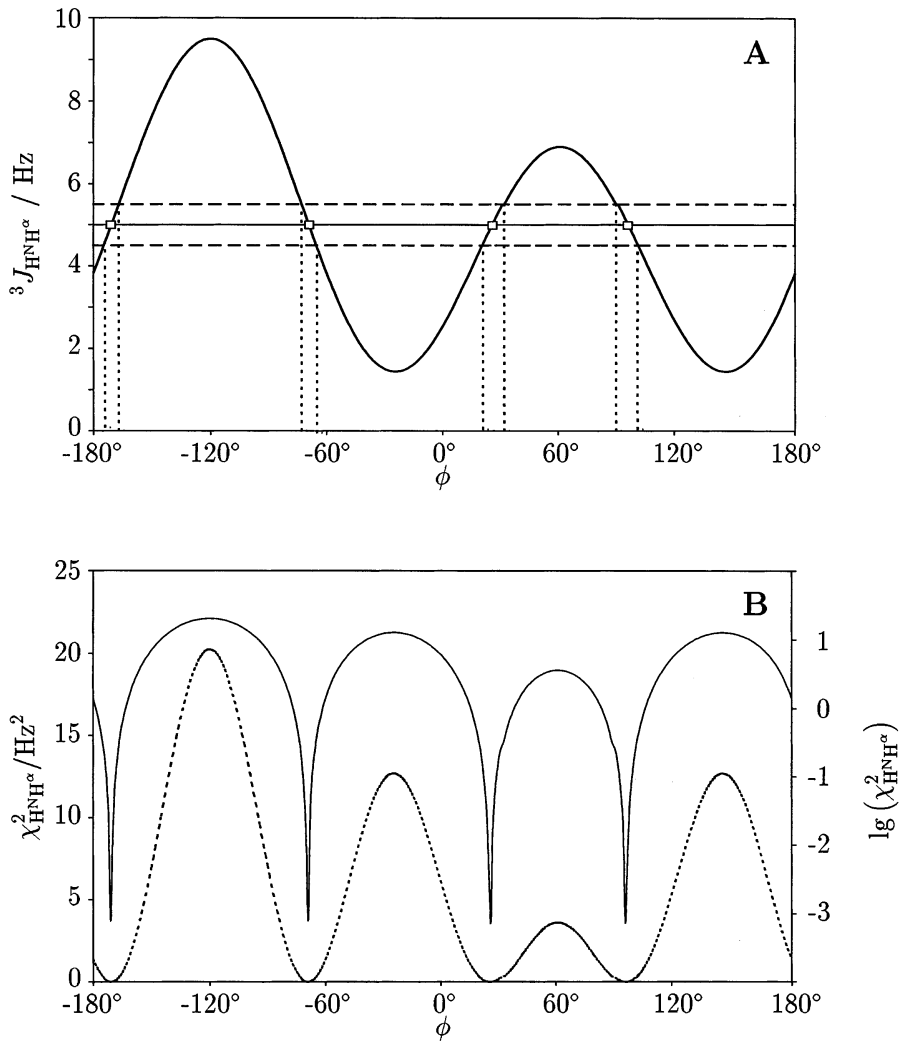

Fig. 2 A Karplus curve using the parameters of Edison et al. (1994) for the $^3J_{H^NH^\alpha}$ coupling. Four possible ϕ dihedral angle solutions may account for an experimental coupling constant of $^3J = 5 \pm 0.5$ Hz as indicated by *vertical bars*. **B** Typical profile of the residual error χ^2 as a function of the ϕ dihedral angle (Eq. (3)) on a linear (*dotted line*) and on a logarithmic scale (*solid line*)

Table 1 Karplus coefficients for the angular dependence of ϕ angle related ^3J coupling constants in polypeptides [a]

θ[°]	^3J coupling	Karplus coefficients [Hz]			Code		$RMSD_J$	Reference
		A	*B*	*C*				
$\phi-60°$	$^3J_{H^NH^\alpha}$	9.4	–1.1	0.4	1		1.18	Bystrov et al. 1973
		5.4	–1.3	2.2	2		0.83	DeMarco et al. 1978
		6.4	–1.4	1.9	3		0.79	Pardi et al. 1984
		6.7	–1.3	1.5	4		0.78	Ludvigsen et al. 1991
		6.51	–1.76	1.60	5		0.80	Vuister & Bax 1993
		6.40	–1.54	1.65	6	*	0.77	Edison et al. 1994
		6.64	–1.43	1.86	7		0.83	Wang & Bax 1996
		6.98	–1.38	1.72	8		0.85	Wang & Bax 1996
$\phi\pm180°$	$^3J_{H^NC'}$	5.7	–2.7	0.1	a		1.00	Solkan & Bystrov 1974
		4.02	–1.12	0.07	b	*	0.45	Wang & Bax 1996
		4.32	–0.84	0.00	c		0.46	Wang & Bax 1996
$\phi+60°$	$^3J_{H^NC^\beta}$	4.7	–1.5	–0.2	i		0.55	Solkan & Bystrov 1974
		2.78	–0.37	0.03	ii		0.36	Wang & Bax 1996
		3.39	–0.94	0.07	iii	*	0.35	Wang & Bax 1996
$\phi+120°$	$^3J_{C'_{i-1}H^\alpha}$	4.5	–1.3	–1.2	I		1.60	Solkan & Bystrov 1974
		9.0	–4.4	–0.8	II		1.39	Bystrov et al. 1975
		3.96	–1.83	–0.8	III		1.84	Kao & Barfield 1985
		3.62	–2.11	1.29	IV		0.41	Wang & Bax 1996
		3.75	–2.19	1.28	V	*	0.40	Wang & Bax 1996
$\phi\pm0°$	$^3J_{C'_{i-1}C'_i}$	2.0	–0.8	–0.3	α		0.82	Solkan & Bystrov 1974
		1.33	–0.88	0.62	β	*	0.35	Hu & Bax 1996 a
$\phi-120°$	$^3J_{C'_{i-1}C^\beta}$	1.5	–0.6	–0.1	*A*		1.29	Solkan & Bystrov 1974
		1.84	–0.23	0.51	*B*		0.80	Kao & Barfield 1985
		1.59	–0.67	0.27	*C*		0.84	Hu & Bax 1996 b
		2.54	–0.55	0.37	*D*	*	0.33	Löhr et al. 1997

[a] Coefficients *A*, *B* and *C* were used with Eq. (1). The various coefficients collected from the literature were adapted to strictly follow the definition of the ϕ dihedral angle according to the IUPAC-IUB convention (1970). To allow quick referencing, the parameter sets are labelled with a unique enumeration scheme. The parameter sets indicated by asterisks were used in the final analysis as they yielded the smallest $RMSD_J$

itio calculations or from correlating experimental coupling constants and dihedral angles in crystal structures. Commonly used Karplus coefficients are given in Table 1. Of particular interest is the influence of the different available coefficients on the transformation of ^3J coupling information into ϕ torsion-angle constraints. Further questions address the combination of ^3J coupling-constant types minimally required for reliable torsion-angle geometry.

The present work aims at predicting accurate backbone ϕ torsion angles in *Desulfovibrio vulgaris* flavodoxin (Mayhew and Tollin 1992) based *exclusively* on *J*-coupling information. The protein chain consists of 147 amino acid residues (the recombinant form aligns with residues 2 through 148 of the native sequence) with a molecular mass of 16.3 kDa (Dubourdieu and Fox 1977). It is a member of a group of small microbial electron-transfer proteins containing non-covalently bound FMN as the redox-active group (Ghisla and Massey 1989). Flavodoxins are known to interact with other redox proteins although the mechanism of electron transfer is yet unknown. Flavodoxin folds according to the frequently encountered β-α-β motif (Chothia 1984), which features a twisted five-stranded parallel β-sheet (residues 3–9, 32–36, 52–58, 86–93, and 124–127) flanked by pairs of α-helices (residues 13–28, 69–76, and 104–114, 134–148) on either face. Recently, the crystal structure of oxidized *D. vulgaris* flavodoxin has been determined with 170 pm resolution (Walsh, unpublished data). The solution structure has also been refined on the basis of 1350 interproton distances from homonuclear and heteronuclear NOESY spectra (Knauf et al. 1993, 1996). To avoid circular argumentation only the refined X-ray conformation will be used as reference structure in the *J* analysis.

Materials and methods

Determination of three-bond coupling constants

Recombinant flavodoxin enriched in the ^{15}N isotope and ^{13}C, ^{15}N doubly labeled flavodoxin were purified according to previously reported protocols (Curley et al. 1988, 1991). For NMR experiments, the protein samples were dissolved to a final concentration of 4.5 mM (^{15}N labeled) and 1.4 mM ($^{13}C/^{15}N$ labeled), respectively, in 0.5 ml 10 mM potassium-phosphate buffer, pH 7, containing 5% D_2O.

Unless otherwise stated, NMR experiments were performed on a Bruker DMX-600 spectrometer equipped with a three-axes pulsed-field gradient (PFG) 5-mm ^1H {^{13}C, ^{15}N} triple-resonance probe. The temperature was 300 K in all experiments.

$^3J_{H^N H^\alpha}$ coupling constants were evaluated utilizing the *J* modulation method (Neri et al. 1990; Billeter et al. 1992) by the water-flip-back 2D *ct*-HMQC-J experiment (Kuboniwa et al. 1994) combined with the WATERGATE solvent-suppression scheme (Piotto et al. 1992). (N, H ^{N}) cross-peak intensities from a series of 13 spectra, recorded with dephasing periods Δ ranging from 44.8 ms to 248.8 ms, were used in a Simplex fit (Nelder and Mead 1965) of the *J* dependent modulation according to Kuboniwa et al. (1994):

$$I(\Delta) = I(0) \exp\left[-\frac{\Delta}{T_{2,\mathrm{MQ}}} - \frac{\Delta}{T_{1,\alpha}} \right] \cdot \left[\cos(\pi J^r \Delta) + \frac{\sin(\pi J^r \Delta)}{2\pi J^r T_{1,\alpha}} \right] \quad (2)$$

with $J^r = (J_{HH}^2 - 1/(2\pi T_{1,\alpha})^2)^{1/2}$. Note, that the constant number of t_1 increments in all spectra allows disregarding the factor N_1 in the original equation. Selective $T_{1,\alpha}$ relaxation times required to account for H^α spin-flip effects were determined from the exponential decay of the ($^1H^\alpha$, $^{13}C^\alpha$) autocorrelation signals (Peng and Wagner 1992) in a series of 2D *ct*-^{1}H {^{13}C}-HSQC-NOESY experiments with mixing times from 35 to 280 ms.

The majority of $^3J_{H^N C'}$ coupling constants were extracted from a 3D heteronuclear relayed E. COSY spectrum (Schmidt et al. 1996) using iterative nonlinear least-squares fitting of 2D multiplet projections including a detailed error analysis. Additional values were measured in three-dimensional (H)CANNH spectra (Löhr and Rüterjans 1995) in combination with procedures to align 1D multiplet-traces (Schwalbe et al. 1993). Both experiments were carried out on a Bruker AMX-600 spectrometer without PFG accessory, using a 2.2 mM sample of doubly labeled *D. vulgaris* flavodoxin.

$^3J_{H^N H^\beta}$ coupling constants were obtained at 600 MHz from a 3D C^β coupled (H)CANNH spectrum as described previously (Löhr and Rüterjans 1995), slightly modified to include gradient-coherence selection and sensitivity enhancement (Kay et al. 1992; Schleucher et al. 1994). In addition, a HNHB spectrum (Archer et al. 1991) was recorded on the doubly labeled sample, exploiting $^1J_{H^\beta C^\beta}$ splittings in the indirectly detected ^{1}H dimension to obtain E. COSY like multiplet patterns, as suggested by Seip et al. (1994). The pulse sequence was based on the version of Madsen et al. (1993), supplemented with gradient-coherence selection and a cosine-modulated G3 pulse applied to ^{13}C nuclei in order to refocus undesired splittings due to $^{13}C'$, ^{15}N and $^{13}C^\alpha$, ^{15}N couplings during the ^{15}N evolution time. The $^{13}C^\beta$ coupled HNHB experiment was performed on a Bruker DRX-800 spectrometer, using a 5 mm quadruple-resonance ^{1}H {^{31}P, ^{13}C, ^{15}N} probe.

Vicinal $^3J_{C'_{i-1}H_i^\alpha}$ coupling constants were extracted from a H^α coupled H(N)CA,CO experiment (Löhr et al. 1997) and from a PFG-based variant of the $^{13}C'$ coupled (H)NCAHA experiment (Löhr and Rüterjans 1995).

Both carbon-carbon coupling constants $^3J_{C'_{i-1}C'_i}$ and $^3J_{C_{i-1}C^\beta}$ were measured in closely related E. COSY versions of the H(N)CA,CO experiment (Löhr et al. 1997). At first, $^{13}C^\alpha$ pulses are band-selective G3 and G4 Gaussian cascades (Emsley and Bodenhausen 1990) in order to avoid perturbation of $^{13}C^\beta$ spin states. The $^1J_{C^\alpha C^\beta}$ coupling then gives rise to a splitting of the multiplets in the $^{13}C^\alpha$ dimension, while the $^3J_{C'_{i-1}C_i^\beta}$ coupling constants were extracted from the displacement of the two multiplet components in the $\omega(^{13}C')$ domain. The second experiment employs a $^{13}C^\alpha$ constant-time evolution period to remove multiplet splittings due to the $^1J_{C^\alpha C^\beta}$ coupling while resolving the passive $^1J_{C^\alpha C'}$ splitting. Application of a small-flip-angle pulse for excitation of $^{13}C'$ spins provides E. COSY type multiplet patterns from which the homonuclear $^3J_{C'_{i-1}C'_i}$ coupling constants were determined.

All E. COSY data sets were processed with the FELIX software (version 1.1 Hare Research, Inc., Woodinville, USA). Accurate ^3J coupling constants were extracted by a computer-assisted trace-alignment procedure (Schmidt et al. 1995) to avoid the limitations due to finite frequency intervals. The coupling constants are listed in Table 2. In cases where multiple determinations were made due to different experimental approaches, those values with the tighter error margins were selected.

Optimization of ϕ torsion geometries

In high-resolution conformational analysis on the basis of ^3J coupling information, the assumption of a single rotameric state for the dihedral-angle orientation is not always justified because internal motion might have led to an averaging of the observed ^3J coupling constants (Jardetzky 1980; Hoch et al. 1985). Hence, distributions in the dihedral-angles must be adjusted in order to minimize the objective function, also termed *J* residual (Schmidt 1997),

$$\varepsilon_J^2 = \sum_k \sigma_k^{-2} \left\{ J_k^{\mathrm{expt}} - \langle J_k^{\mathrm{calc}} \rangle \right\}^2 = \sum_k \sigma_k^{-2} \left\{ J_k^{\mathrm{expt}} - \sum_l \left[p(\theta_l)\, J_k^{\mathrm{calc}}(\theta_l) \right] \right\}^2 \quad (3)$$

where *k* denotes the different *J* coupled spin pairs and *l* runs over the considered dihedral-angle conformations. J^{expt} and J^{calc} are the experimental *J* coupling constants and those calculated from a molecular model, respectively. The contribution from the particular coupling constant J_k to the error is properly weighted by its specific experimental uncertainty σ_k. Any solution to the probability profile $p(\theta)$, that makes the residual fall below a given threshold, e. g., the sum of variances (squared experimental uncertainties) of the experimental *J* coupling constants, is considered to fulfill a set of experimental *J* coupling constraints. In this concept, different models of internal dynamics express as different probability-distribution profiles $p(\theta)$. Simple motional models are applied to discover the most probable distribution of rotameric states (Schmidt

1997) according to (i) a peaked distribution associated with a single rigid conformation, (ii) a Gaussian distribution about a mean dihedral angle or (iii) a two state jump model. The known standard deviations in the experimental J coupling constants were propagated into confidence bounds on the fit parameters using weight-matrix techniques (Clifford 1973). Considering the varying number of degrees of freedom in the different models, the significance measures emerge from an analysis of variance ratios retrieved from Fisher's F distribution using the critical value $1-\alpha=0.84$ for a two-tailed test (Sokal and Rohlf 1981; Waits 1994).

X-ray reference structure

The results of the NMR-based dihedral-angle analysis are compared to the X-ray structure with 170 pm resolution (Martin Walsh, private communication). Reference ϕ dihedral angles were derived twice, firstly, from heavy-atom coordinates $\phi_{C'_{i-1}C'_i} = \theta(C'_{i-1} - N - C^{\alpha} - C'_i)$ (IUPAC-IUB, 1970), and secondly, from $\phi_{C'_{i-1}C^{\beta}} = \theta(C'_{i-1} - N - C^{\alpha} - C^{\beta}) + 120°$. The two methods revealed that the $C'_i - C_i^{\alpha} - C_i^{\beta}$ bond angle is only slightly distorted, in agreement with Laskowski and Moos (1993), with an average difference $\Delta\phi = \phi_{C'_{i-1}C'_i} - \phi_{C'_{i-1}C^{\beta}} = 0.6°$ and a distribution of ±4.0°. Hence both sets were conveniently averaged to account for deviations from ideal bonding geometry.

Results and discussion

Vicinal coupling constants related to the backbone ϕ torsion angles in *Desulfovibrio vulgaris* flavodoxin have been determined by a variety of heteronuclear 2D and 3D NMR experiments. Quantitative evaluations including confidence bounds were accomplished for 124 $^3J_{H^NH^{\alpha}}$, 123 $^3J_{H^NC'_i}$, 118 $^3J_{H^NC^{\beta}}$, 117 $^3J_{C'_{i-1}H^{\alpha}}$, 109 $^3J_{C'_{i-1}C'_i}$, and 103 $^3J_{C'_{i-1}C^{\beta}}$ coupling constants. Complete sets comprising all six possible coupling constants are available for 88 out of 126 non-glycine and non-proline amino-acid residues, while for 20, 9, and 6 further residues, smaller sets comprising 5, 4, and 3 coupling constants, respectively, were obtained. A summary of the experimental constraints is given in Table 2.

Selection of Karplus parameters for the ϕ related ^3J couplings

The diverse Karplus parametrizations for the ϕ related couplings found in the literature are compiled in Table 1. To estimate the effective impact of variations in the critical coefficients on the J values predicted from a model geometry pairwise root-mean-square differences (RMSD) between either two Karplus curves m and n were computed according to

$$\mathrm{RMSD}_{m,n} = \left[\frac{1}{2\pi} \int_{-\pi}^{+\pi} \{(A_m - A_n)\cos^2\theta + (B_m - B_n)\cos\theta + (C_m - C_n)\}^2 \, d\theta \right]^{\frac{1}{2}}$$
$$= \left[\frac{3}{8}(A_m - A_n)^2 + \frac{1}{2}(B_m - B_n)^2 + (C_m - C_n)^2 + (A_m - A_n)(C_m - C_n) \right]^{\frac{1}{2}}. \quad (4)$$

In particular, the parametrization of the $^3J_{H^NH^{\alpha}}$ coupling has long been a focus of interest, as it was the first coupling to be measured at natural isotope abundance. The eight available sets of coefficients are depicted in Fig. 3 a. Curve 1 (Bystrov 1976) exhibits the largest amplitude, while curve 2 (DeMarco et al. 1978) is flattest. The largest and smallest RMSD between either two curves are 1.44 Hz and 0.13 Hz, respectively, as summarized in Table 3. Note that the latter deviation is in the range of the experimental uncertainty of the coupling constants.

The parametrizations for the heteronuclear $^3J_{H^NC'}$, $^3J_{H^NC^{\beta}}$, and $^3J_{C'_{i-1}H^{\alpha}}$ coupling constants diverge considerably, as depicted in Fig. 3 b–d. The maximum discrepancies found within the sets of curves are 1.61, 1.28 and 3.79 Hz, respectively. However, recent empirical parametrizations for the homonuclear C-C couplings (Hu and Bax 1996 a, b; Löhr et al. 1997) agree with those predicted on the basis of FPT-INDO calculations (Solkan and Bystrov 1974), as demonstrated in Fig. 3 e, f. The respective maximal RMSD values are 0.63 Hz for $^3J_{C'_{i-1}C'_i}$ and 0.40 Hz for $^3J_{C'_{i-1}C^{\beta}}$.

In order to pick the optimal Karplus parameter sets for use in the J coupling analysis, dihedral angles and coupling constants were referenced from only those residues likely to adopt rigid conformations as part of secondary structure. In total, ϕ angles from 48 residues in the α-helices and β-strands were selected, excluding the terminal residues and loop regions, to back-calculate the set of coupling constants using each of the Karplus parameter sets listed in Table 1. For comparison with experiment, *r.m.s.* deviations with respect to all J values participating in the selection were calculated according to

$$\mathrm{RMSD}_J = \left[\frac{1}{48} \sum_{i=1}^{48} (J_i^{\mathrm{expt}} - J_i^{\mathrm{calc}})^2 \right]^{\frac{1}{2}}. \quad (5)$$

Karplus parameters for the further analysis were chosen based on minimal violation as indicated in Table 1. Parametrizations for $^3J_{H^NC'_i}$, $^3J_{H^NC^{\beta}}$, $^3J_{C'_{i-1}H^{\alpha}}$ and $^3J_{C'_{i-1}C'_i}$ calibrated with ubiquitin (Wang and Bax 1996; Hu and Bax 1996) were most appropriate. For $^3J_{H^NH^{\alpha}}$, the parameters as derived from *ab-initio* calculations by Edison et al. (1994), yielded the smallest RMSD_J value. No satisfactory results were obtained for $^3J_{C'_{i-1}C^{\beta}}$, as all existing parametrizations predict the majority of the coupling constants to be considerably smaller than our experimental values. Therefore, this particular coupling was recently parametrized based on flavodoxin data (Löhr et al. 1997).

Table 2 Results of the ϕ dihedral angle analysis in *Desulfovibrio vulgaris* flavodoxin

Residue		Experimental/Back-calculated coupling constants [Hz]						ϕ Torsion [deg]	
		$^3J_{H^NH^\alpha}$	$^3J_{H^NC'}$	$^3J_{H^NC^\beta}$	$^3J_{C'_{i-1}H^\alpha}$	$^3J_{C'_{i-1}C'}$	$^3J_{C'_{i-1}C^\beta}$	NMR	X-ray
Lys	3	9.58/9.41	0.18/0.18	0.91/0.90	3.10/2.77	0.74/1.10	1.64/1.63	–110.9	–107.0
Ala	4	9.83/9.59	0.97/0.53	0.62/0.53	2.81/2.84	1.41/1.40	1.56/1.19	–120.3	–120.3
Leu	5	8.95/8.86	0.67/0.67	0.88/0.76	2.56/2.58	1.78/1.37	1.63/1.40	–117.6±11.0	–113.5
Ile	6	9.63/9.43	1.15/0.94	0.19/0.26	3.38/2.78	2.11/1.69	1.19/0.85	–128.6	–119.2
Val	7	9.81/9.52	0.93/0.78	n. a.	2.89/2.81	n. a.	n. a.	–125.6	–119.8
Tyr	8	9.51/9.45	0.91/0.91	–0.04/0.28	3.44/2.79	1.55/1.67	0.73/0.88	–128.0	–131.5
Ser	10	8.42/8.54	1.79/1.71	n. a.	2.83/2.46	2.04/2.15	n. a.	–142.4	–142.2
Thr	11	8.29/8.44	–0.59/–0.01	n. a.	2.79/2.42	n. a.	n. a.	–96.5	–93.3
Thr	12	9.61/9.43	0.32/0.19	0.87/0.89	3.00/2.78	0.64/1.12	n. a.	–111.3	–106.0
Asn	14	4.44/4.63	0.80/1.26	2.42/2.42	1.90/1.26	n. a.	3.63/3.26	–65.0	–70.6
Glu	16	5.34/5.42	0.32/0.86	2.51/2.35	0.76/1.46	0.05/0.47	2.89/3.18	–71.0	–67.9
Tyr	17	3.48/3.65	1.70/1.89	2.45/2.43	n. a.	0.25/0.54	3.54/3.27	–56.8	–60.5
Thr	18	n. a.	1.63/1.75	n. a.	0.86/1.09	0.73/0.52	n. a.	–58.5	–58.7
Ala	19	4.27/4.13	1.61/1.57	3.10/2.44	0.68/1.14	0.64/0.51	3.80/3.28	–60.9	–59.2
Glu	20	4.17/4.14	1.66/1.56	1.98/2.44	1.30/1.15	0.53/0.51	3.28/3.28	–61.0	–68.7
Thr	21	4.94/4.93	1.17/1.10	n. a.	1.45/1.33	0.56/0.48	n. a.	–67.3	–65.7
Ile	22	5.39/4.97	1.31/1.08	2.11/2.39	0.24/1.34	0.02/0.48	3.77/3.23	–67.6	–61.5
Ala	23	3.39/3.25	2.60/2.18	3.10/2.40	1.53/1.00	0.82/0.57	3.98/3.24	–53.2	–56.3
Arg	24	4.53/4.46	1.55/1.36	2.29/2.43	1.40/1.22	0.55/0.49	3.44/3.27	–63.6	–64.2
Glu	25	4.96/4.96	n. a.	2.88/2.40	1.50/1.34	n. a.	n. a.	–67.5	–65.3
Leu	26	5.23/5.33	1.09/0.90	2.19/2.36	2.00/1.43	0.50/0.47	3.04/3.19	–70.4	–67.2
Ala	27	4.05/4.26	1.30/1.48	2.54/2.44	1.76/1.17	0.77/0.50	3.54/3.28	–62.0	–65.8
Asp	28	4.53/4.59	1.47/1.29	2.41/2.42	1.83/1.25	0.17/0.49	2.94/3.26	–64.6±17.4	–66.4
Ala	29	7.91/7.90	0.28/0.20	2.00/1.63	2.48/2.25	0.95/0.73	2.37/2.43	–92.9±12.3	–82.2
Tyr	31	6.97/6.90	–0.15/0.28	2.12/2.06	1.31/1.90	0.77/0.53	2.91/2.88	–82.5	–71.1
Glu	32	8.65/8.48	0.10/–0.01	0.98/1.51	2.55/2.44	0.83/0.74	3.25/2.30	–96.9	–94.3
Val	33	9.29/9.46	0.31/0.22	1.26/0.85	2.87/2.79	1.67/1.14	1.50/1.57	–112.2	–116.2
Asp	34	9.49/9.59	0.94/0.56	0.46/0.50	2.82/2.84	1.51/1.43	1.66/1.16	–121.1	–118.3
Ser	35	9.45/9.47	0.58/0.23	1.23/0.83	2.87/2.80	1.33/1.15	n. a.	–112.6	–107.2
Arg	36	9.03/9.20	0.90/1.20	0.36/0.15	3.28/2.70	2.40/1.86	0.94/0.69	–133.5	–128.6
Asp	37	6.72/6.62	0.21/0.37	2.41/2.13	1.66/1.81	–0.19/0.51	2.96/2.96	–80.3	–67.4
Ala	38	3.27/3.21	2.53/2.22	2.63/2.40	1.12/0.99	–0.11/0.57	4.14/3.24	–52.8	–61.4
Ala	39	4.50/4.30	1.53/1.46	2.53/2.44	0.61/1.18	n. a.	4.07/3.28	–62.3	–58.4
Ser	40	8.99/8.89	0.13/0.01	1.79/1.30	2.83/2.58	1.13/0.86	n. a.	–101.8	–94.5
Val	41	8.87/8.92	0.30/0.01	1.45/1.28	2.82/2.59	0.74/0.87	1.94/2.05	–99.5±17.4	–112.1
Glu	42	8.73/8.65	0.65/0.52	1.04/0.94	2.59/2.56	1.24/1.14	1.80/1.70	–127.0 & –94.4	–110.5
Ala	43	3.59/3.82	1.63/1.77	2.60/2.44	1.73/1.09	0.43/0.52	3.94/3.28	–60.6±20.8	–64.4
Leu	46	2.58/2.59	3.40/2.76	2.78/2.30	1.29/0.96	0.06/0.65	3.03/3.13	–46.4±10.7	–49.9
Phe	47	6.73/6.89	0.10/0.29	1.64/2.06	2.16/1.90	–0.36/0.53	2.82/2.89	–82.4±11.9	–86.7
Glu	48	3.80/4.04	1.37/1.64	2.29/2.43	1.40/1.14	0.25/0.52	3.13/3.27	–60.1±17.0	–61.2
Phe	50	8.67/8.89	–0.17/0.01	1.33/1.30	2.62/2.58	0.43/0.85	1.49/2.07	–101.8	–106.8
Asp	51	6.76/7.24	–1.10/0.19	1.59/1.97	2.23/2.01	0.05/0.56	2.72/2.79	–85.3	–88.3
Leu	52	6.53/7.00	1.60/2.43	–0.28/0.11	2.13/1.94	2.24/2.55	0.23/0.34	–156.7	–141.4
Val	53	9.00/9.51	0.35/0.28	1.16/0.77	3.66/2.81	1.78/1.20	1.47/1.48	–114.0	–123.2
Leu	54	9.91/9.59	0.60/0.50	0.76/0.55	3.20/2.84	1.34/1.38	1.13/1.22	–119.7	–113.3
Cys	57	6.75/7.50	1.91/2.24	–0.02/0.05	1.93/2.10	n. a.	0.19/0.34	–152.5	–159.0
Ser	58	7.52/7.55	0.10/0.11	n. a.	2.31/2.12	0.31/0.59	n. a.	–88.0	–85.4
Thr	59	9.84/9.36	0.06/0.15	n. a.	2.08/2.76	0.70/1.07	n. a.	–109.8	–109.2
Trp	60	9.64/9.29	1.56/1.11	0.00/0.19	3.58/2.73	2.34/1.80	1.19/0.74	–131.8	–125.4
Asp	62	7.42/5.80	1.66/1.13	2.18/1.51	n. a.	–0.02/6.59	1.43/0.59	67.9±19.1	70.2
Ser	64	6.55/6.57	2.66/2.25	0.66/0.42	2.49/1.88	2.32/2.44	n. a.	–159.2±17.1	–150.6
Ile	65	6.80/6.73	1.02/0.70	2.12/1.83	2.54/1.93	0.58/0.70	2.82/2.63	–83.5±20.9	–91.3
Glu	66	9.79/9.57	2.07/0.65	0.17/0.44	3.28/2.83	1.58/1.49	1.68/1.08	–123.0	–120.0
Leu	67	5.60/5.98	0.24/0.61	1.11/2.26	0.98/1.62	n. a.	3.52/3.09	–73.6	–79.4
Gln	68	3.01/3.16	2.30/2.26	3.11/2.39	0.87/0.99	0.71/0.58	4.00/3.23	–52.3	–49.4
Asp	69	2.33/2.53	n. a.	2.06/2.28	0.93/0.96	n. a.	4.04/3.11	–45.6	–50.8
Asp	70	5.74/5.89	0.09/0.65	2.11/2.28	1.55/1.59	0.25/0.48	3.66/3.11	–74.6	–69.9
Phe	71	6.76/7.04	0.07/0.31	2.14/1.97	2.62/1.96	1.02/0.57	2.76/2.79	–83.8±8.9	–84.4
Ile	72	2.49/2.74	2.09/2.61	2.71/2.33	0.69/0.96	0.30/0.63	3.28/3.17	–48.1	–47.9
Leu	74	6.29/6.13	0.52/0.55	2.02/2.23	0.99/1.66	0.73/0.49	3.13/3.06	–76.5±9.6	–62.0
Phe	75	4.17/4.10	1.42/1.59	2.92/2.44	0.48/1.14	0.67/0.51	3.50/3.28	–60.6	–57.8
Asp	76	3.74/3.94	1.48/1.69	2.46/2.44	1.38/1.11	0.40/0.52	3.24/3.28	–59.3	–68.2
Ser	77	9.59/9.37	0.35/0.15	1.29/0.95	n. a.	n. a.	n. a.	–109.9	–103.0
Leu	78	1.21/1.83	3.24/3.69	2.43/1.98	1.54/1.12	n. a.	n. a.	–34.9	–59.1
Glu	79	3.33/3.44	2.05/2.13	2.28/2.35	1.24/1.08	0.07/0.58	3.12/3.19	–54.6±10.1	–59.5
Glu	80	7.05/7.41	–0.30/0.15	1.90/1.92	2.61/2.07	0.42/0.57	2.45/2.73	–86.8	–96.8

Table 2 (Continued)

Residue		Experimental/Back-calculated coupling constants [Hz]						ϕ Torsion [deg]	
		$^3J_{H^NH^\alpha}$	$^3J_{H^NC'}$	$^3J_{H^NC^\beta}$	$^3J_{C'_{i-1}H^\alpha}$	$^3J_{C'_{i-1}C'}$	$^3J_{C'_{i-1}C^\beta}$	NMR	X-ray
Thr	81	5.64/5.80	0.79/0.76	2.48/2.23	2.38/1.59	0.27/0.51	n. a.	–73.9±9.9	–78.9
Ala	83	5.98/5.92	1.21/0.85	2.89/2.11	2.51/1.67	0.30/0.57	2.85/2.93	–75.0±15.3	–82.1
Gln	84	3.29/3.75	1.20/1.82	2.26/2.44	1.00/1.07	–0.02/0.53	3.52/3.28	–57.7	–56.8
Arg	86	6.87/7.05	–0.12/0.24	2.11/2.02	2.20/1.95	0.75/0.54	2.83/2.84	–83.7	–79.1
Lys	87	6.86/6.78	0.34/0.32	2.14/2.09	2.21/1.86	–0.02/0.52	3.45/2.92	–81.5	–82.9
Val	88	9.70/9.49	0.89/0.85	0.39/0.31	2.96/2.80	2.02/1.63	1.06/0.92	–126.9	–133.4
Ala	89	6.23/6.30	3.27/2.65	0.00/0.23	2.36/1.72	2.74/2.66	0.25/0.37	–162.2	–153.1
Cys	90	9.73/9.51	–0.07/0.28	1.24/0.78	3.30/2.81	1.69/1.19	1.39/1.49	–113.9	–120.6
Phe	91	8.35/8.27	2.06/1.87	–0.25/0.02	2.50/2.37	2.21/2.24	0.27/0.41	–145.3	–147.7
Cys	93	9.60/9.31	0.12/0.12	1.57/1.00	3.32/2.74	n. a.	n. a.	–108.6	–105.1
Asp	95	8.01/8.05	1.94/1.99	0.17/0.02	2.63/2.29	2.67/2.31	0.39/0.38	–147.5	–149.3
Ser	96	4.75/5.01	1.05/1.06	2.44/2.39	2.31/1.35	–0.21/0.48	n. a.	–67.9	–65.5
Ser	97	7.03/7.02	0.31/0.29	2.02/2.00	n. a.	n. a.	n. a.	–83.4±7.7	–76.4
Tyr	98	8.89/8.43	–0.06/0.00	2.16/1.54	2.01/2.42	0.73/0.73	2.39/2.33	–96.3	–88.3
Glu	99	4.51/4.28	2.04/1.47	2.68/2.44	1.77/1.18	n. a.	n. a.	–62.2	–65.2
Tyr	100	8.00/7.92	1.28/0.77	1.37/1.15	n. a.	0.38/1.17	1.29/1.83	–106.6±11.6	–105.9
Phe	101	3.00/3.35	1.20/2.11	3.27/2.41	1.51/1.01	0.62/0.56	3.69/3.25	–54.1	–63.5
Cys	102	7.06/6.26	3.07/2.63	0.58/0.40	6.93/7.01	n. a.	0.53/0.45	47.9	53.0
Ala	104	5.59/5.46	0.67/0.84	2.15/2.34	0.75/1.47	n. a.	3.41/3.18	–71.4	–61.3
Val	105	4.42/4.72	0.56/1.22	2.06/2.42	0.88/1.28	0.47/0.48	3.23/3.25	–65.6	–61.4
Asp	106	3.86/3.76	1.94/1.81	2.54/2.44	0.88/1.07	0.29/0.53	3.40/3.28	–57.8	–60.4
Ala	107	2.88/3.38	1.57/2.09	2.95/2.42	1.01/1.02	0.40/0.56	3.84/3.25	–54.4	–64.3
Ile	108	6.20/5.94	0.93/0.63	2.61/2.27	1.46/1.61	0.75/0.48	3.30/3.10	–75.0	–67.3
Glu	109	3.28/3.51	1.72/1.98	2.48/2.42	1.10/1.03	0.40/0.55	3.51/3.26	–55.6	–59.5
Glu	110	3.63/3.65	1.88/1.89	2.29/2.43	1.01/1.05	0.47/0.54	3.68/3.27	–56.8	–58.3
Lys	111	5.20/5.20	0.94/0.96	2.41/2.37	n. a.	–0.12/0.48	3.32/3.21	–69.4	–62.0
Leu	112	3.54/3.73	1.43/1.83	2.33/2.44	0.68/1.07	1.01/0.53	3.59/3.27	–57.5	–60.8
Lys	113	4.06/4.16	1.57/1.66	2.27/2.36	1.33/1.21	0.20/0.54	3.13/3.20	–60.8±11.4	–64.3
Asn	114	4.50/4.60	1.30/1.28	2.47/2.42	1.67/1.25	–0.05/0.49	3.37/3.26	–64.7	–73.5
Leu	115	7.82/7.78	0.40/0.15	1.76/1.73	2.39/2.21	0.07/0.67	2.42/2.53	–90.3±9.0	–78.7
Ala	117	6.05/6.00	0.55/0.60	2.12/2.26	1.48/1.62	0.37/0.48	3.35/3.09	–75.5	–67.5
Glu	118	7.25/7.66	0.18/0.46	1.33/1.54	2.93/2.20	0.30/0.83	1.90/2.31	–93.9±20.4	–104.1
Ile	119	6.44/6.50	0.56/0.57	1.89/2.04	1.97/1.81	0.40/0.58	2.92/2.86	–79.4±14.0	–81.9
Val	120	5.71/5.80	1.09/1.00	2.28/2.06	2.49/1.67	0.28/0.61	2.98/2.88	–74.1±19.4	–78.7
Gln	121	6.30/6.32	3.04/2.64	0.20/0.23	2.14/1.72	2.76/2.66	0.16/0.37	–162.0	–150.3
Asp	122	4.60/4.30	1.93/1.53	2.30/2.38	0.69/1.22	0.44/0.52	3.32/3.22	–62.1±10.1	–64.2
Leu	124	7.81/7.85	–0.24/0.06	1.87/1.77	2.83/2.22	0.20/0.63	2.89/2.58	–90.6	–85.0
Arg	125	9.02/9.29	1.06/0.11	1.35/1.01	n. a.	n. a.	1.36/1.75	–108.3	–114.1
Ile	126	8.80/8.74	–0.58/0.00	1.11/1.38	2.64/2.53	1.14/0.81	2.68/2.16	–99.9	–94.1
Asp	127	9.04/8.79	0.46/0.00	1.39/1.35	2.56/2.55	0.69/0.83	2.50/2.13	–100.6	–96.6
Asp	129	3.70/3.99	0.90/1.99	2.43/2.19	2.05/1.32	0.47/0.61	n. a.	–59.9±12.0	–63.4
Arg	131	5.84/5.65	1.20/0.99	1.79/2.14	0.83/1.61	0.81/0.57	3.11/2.96	–73.0±10.6	–63.0
Ala	132	8.04/7.74	0.10/0.08	2.21/1.81	1.93/2.18	0.69/0.61	2.88/2.62	–89.6	–91.1
Ala	133	9.35/9.53	0.63/0.31	1.12/0.73	2.99/2.82	1.27/1.23	1.32/1.44	–114.9	–126.7
Arg	134	2.32/2.26	3.61/3.13	2.16/2.18	1.29/1.00	0.49/0.70	3.56/3.01	–42.0±3.8	–53.1
Asp	135	4.18/4.74	1.14/1.21	2.42/2.41	1.30/1.28	0.69/0.48	3.25/3.25	–65.8±4.7	–64.8
Asp	136	5.96/5.84	0.79/0.67	2.18/2.28	n. a.	0.53/0.48	3.60/3.12	–74.3	–68.7
Ile	137	5.40/5.31	1.05/0.91	2.37/2.36	1.34/1.43	–0.31/0.47	n. a.	–70.2	–68.9
Val	138	4.34/4.27	1.37/1.48	2.91/2.44	0.70/1.17	0.38/0.50	3.76/3.28	–62.0	–59.7
Trp	140	4.96/4.58	1.68/1.30	3.20/2.42	0.97/1.24	0.87/0.49	4.03/3.26	–64.5	–66.7
Ala	141	4.24/4.30	1.57/1.46	2.66/2.44	1.84/1.18	0.36/0.50	3.82/3.28	–62.3	–61.3
His	142	4.60/4.65	1.16/1.25	2.92/2.42	1.41/1.26	0.39/0.49	3.36/3.26	–65.1	–63.6
Asp	143	5.69/5.22	1.22/0.96	2.54/2.37	0.27/1.40	–0.06/0.47	3.42/3.21	–69.5	–63.4
Val	144	4.68/4.64	1.39/1.26	2.47/2.42	1.34/1.26	0.01/0.49	n. a.	–65.0±9.2	–63.9
Arg	145	6.19/5.73	1.74/1.05	2.34/2.05	1.45/1.66	0.02/0.61	3.04/2.87	–73.3±20.1	–62.5
Ala	147	7.35/7.39	0.49/0.45	2.13/1.69	2.41/2.11	0.73/0.74	2.19/2.48	–89.7±18.3	–98.0
Ile	148	8.95/9.07	0.78/0.04	1.17/1.19	2.64/2.65	0.92/0.92	2.02/1.95	–105.4±21.6	–113.2

[a] n. a.: Experimental value not available

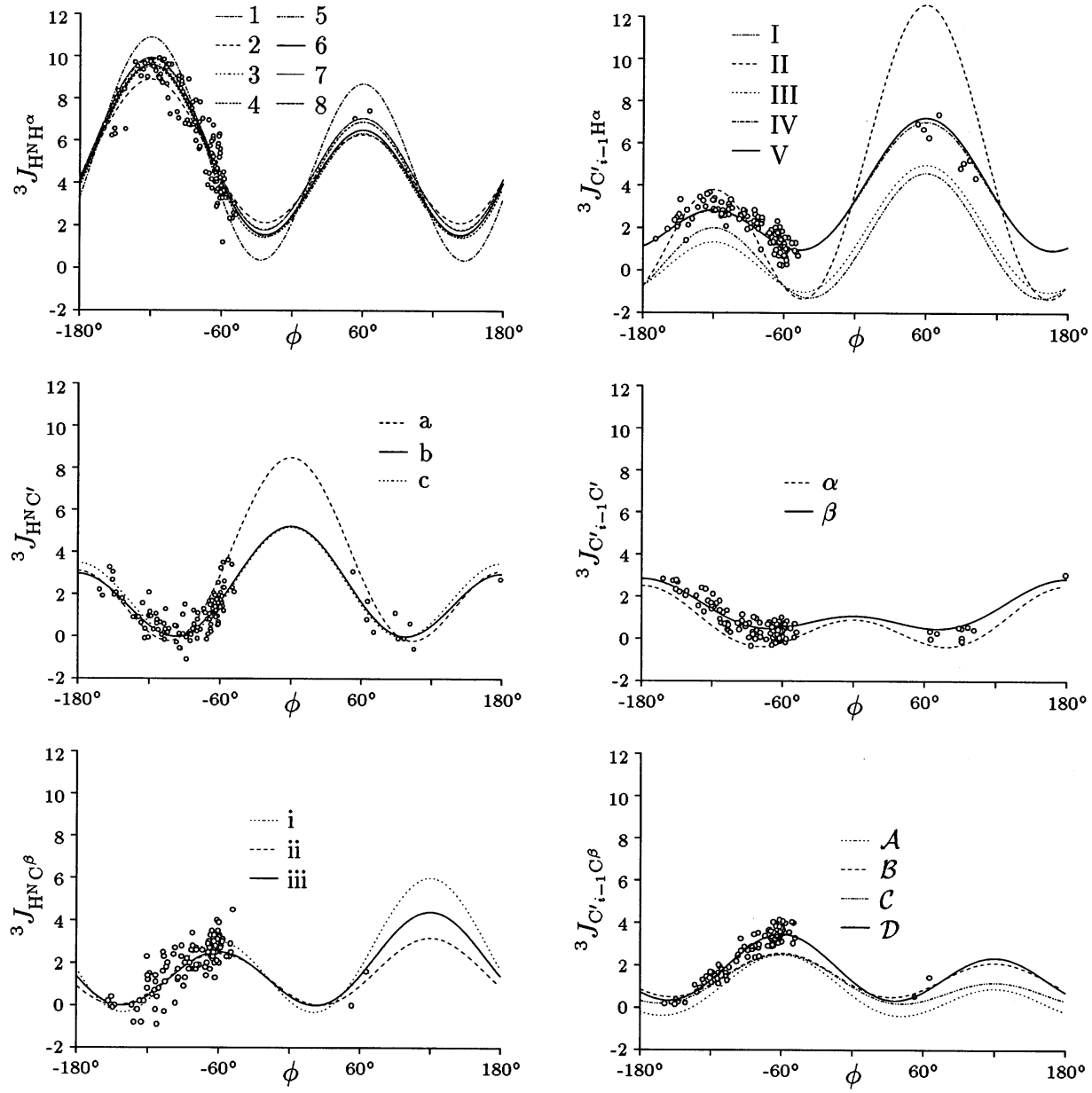

Fig. 3 Angular dependences of homo- and heteronuclear ^3J coupling constants related to the polypeptide-backbone torsion ϕ. Karplus coefficients in Eq. (1) were encoded as given in Table 1. The curves used in the final torsion angle analysis are represented by *solid lines. Circles* represent the experimental coupling constants plotted against ϕ dihedral angles in the X-ray reference structure

There is no real proof for the correctness of one or other of the Karplus parametrizations as long as a fundamental theory for the calculation of *J* couplings is lacking. The rapidly increasing number of high-resolution conformational studies by both X-ray and NMR spectroscopy will provide a larger pool of reference structures that will increase the reliability of the available Karplus parametrizations.

Dihedral-angle ambiguity maps

As shown in Fig. 2, a single coupling usually does not sufficiently determine the corresponding torsion angle. A graphical representation, so-called ambiguity maps, shall be introduced to be able to assess the even more complicated situation with multiple *J* coupling constants considered. The two-dimensional self-correlation diagram of a Karplus curve reveals dihedral-angle regions, the determination of which remains ambiguous with respect to a single coupling constant applied (Fig. 4). The actual shape of a constituent single-coupling ambiguity map depends on both the phase and the magnitude of the Karplus curve for the associated coupling. This is illustrated in Fig. 4 for the six individual coupling constants connected to the ϕ dihedral angle in polypeptides.

Table 3 Expected discrepancy (Hz) in the $^3J_{H^NH^\alpha}$, $^3J_{H^NC'_i}$, $^3J_{H^NC^\beta}$, $^3J_{C'_{i-1}H^\alpha}$, and $^3J_{C'C^\beta}$ coupling constants from different applied sets of Karplus coefficients [a]

$^3J_{H^NH^\alpha}$	1	2	3	4	5	6	7	8
1	0	1.44	1.08	1.00	1.15	1.13	1.01	0.89
2	1.44	0	0.41	0.46	0.51	0.40	0.53	0.64
3	1.08	0.41	0	0.28	0.36	0.27	0.12	0.23
4	1.00	0.46	0.28	0	0.33	0.20	0.34	0.38
5	1.15	0.51	0.36	0.33	0	0.16	0.40	0.48
6	1.13	0.40	0.27	0.20	0.16	0	0.35	0.43
7	1.01	0.53	0.12	0.34	0.40	0.35	0	0.13
8	0.89	0.64	0.23	0.38	0.48	0.43	0.13	0

$^3J_{H^NC'}$	a	b	c
a	0	1.54	1.61
b	1.54	0	0.24
c	1.61	0.24	0

$^3J_{C'H^\alpha}$	I	II	III	IV	V
I	0	3.79	1.78	2.15	2.21
II	3.79	0	2.71	2.57	2.49
III	1.78	2.71	0	0.40	0.46
IV	2.15	2.57	0.40	0	0.09
V	2.21	2.49	0.46	0.09	0

$^3J_{H^NC^\beta}$	i	ii	iii
i	0	1.28	0.72
ii	1.28	0	0.57
iii	0.72	0.57	0

$^3J_{C'C^\beta}$	*A*	*B*	*C*	*D*
A	0	0.84	0.40	0.98
B	0.84	0	0.49	0.40
C	0.40	0.49	0	0.67
D	0.98	0.40	0.67	0

[a] Off-diagonal entries are averages due to a rotation of the ϕ torsion angle over the complete 2π interval according to Eq. (4) in the text. Parameter sets are coded as defined in Table 1

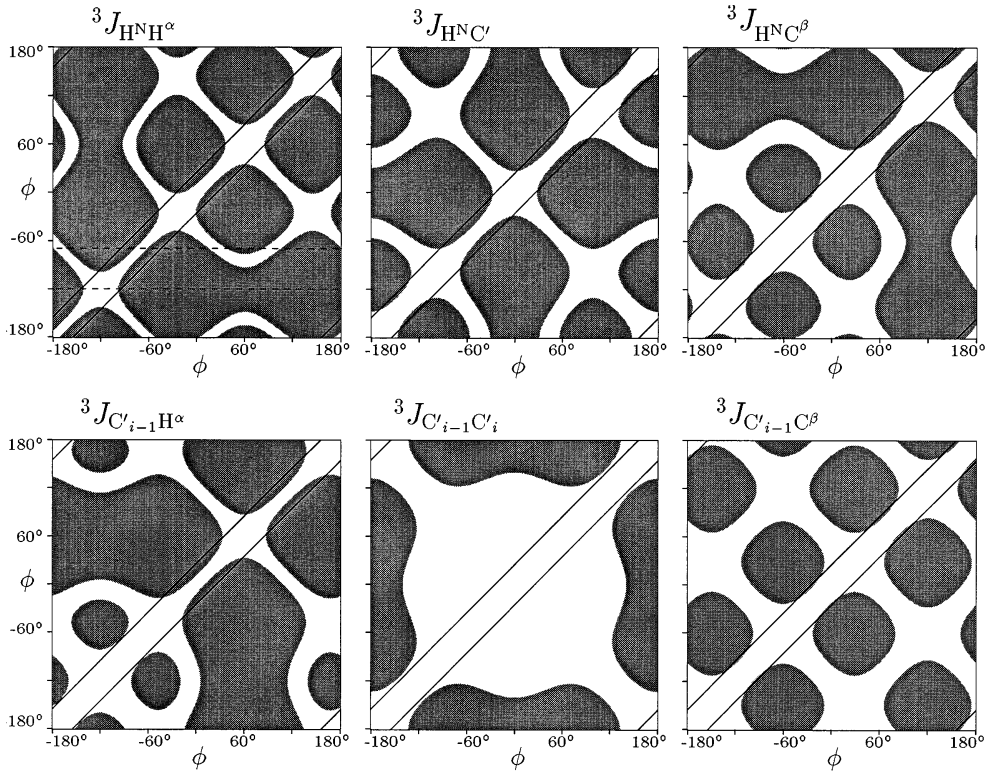

Fig. 4 Dihedral-angle ambiguity maps for the exclusive use of each of the ϕ related J coupling constants. Graphs are prepared for an experimental precision of ±0.5 Hz with those Karplus parameters marked with *asterisks* in Table 1. Two conformations ϕ_1 and ϕ_2 whose associated coupling constants differ by less than 1 Hz give rise to unresolvable (ϕ, ϕ) regions indicated in *white*, otherwise (ϕ, ϕ) dihedral angle pairs, that can be distinguished by the single respective ^3J coupling, are represented in *grey. Diagonal lines* indicate a coincidence region of $\Delta\phi$ ±25°. The *dotted lines* in the $^3J_{H^NH^\alpha}$ map are examples described in the text

The dotted line at ϕ=–120° in the $^3J_{H^NH^\alpha}$ ambiguity map intersects with a broad indiscriminable dihedral-angle range of 50° (white) centered at (ϕ, ϕ) = (–120°, –120°). This situation represents a coupling constant of 9.5±0.5 Hz and thus reflects the broad maximum of the Karplus curve in Fig. 2. The rest of the parallel hits grey regions only, indicating dihedral angles, which can be distinguished from –120°, since any expected $^3J_{H^NH^\alpha}$ coupling constant is smaller than 9.0 Hz. The dotted line at a ϕ dihedral angle of approximately –70° represents the situation described

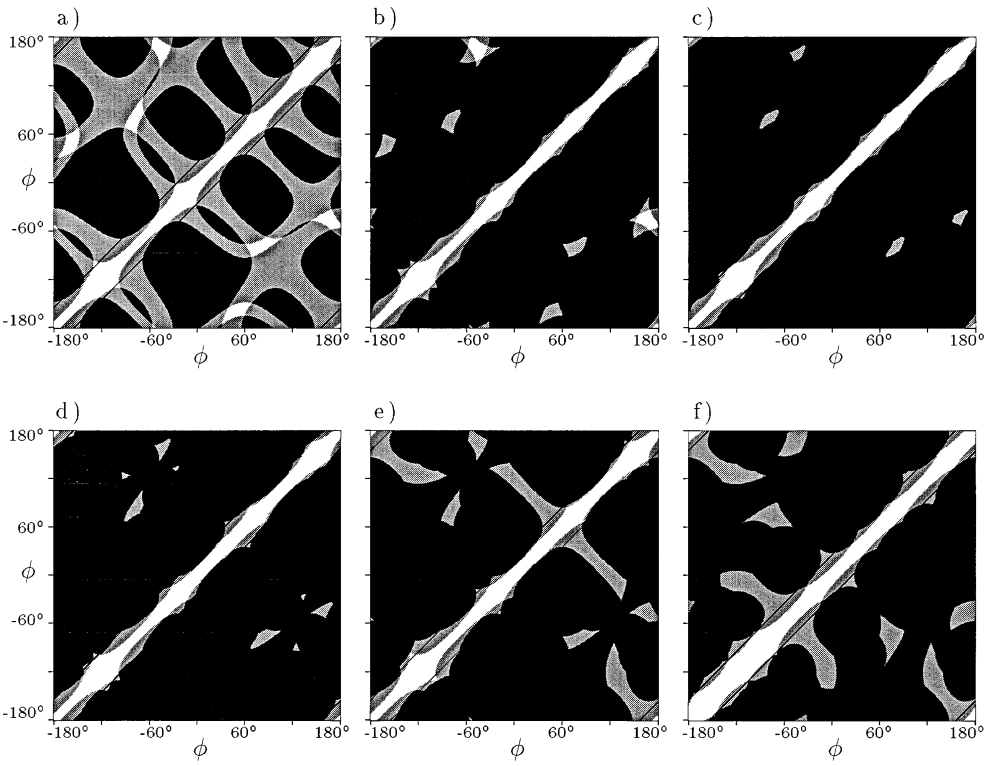

Fig. 5 a–f Dihedral-angle ambiguity maps for *combinations* of ϕ related coupling constants: **a** $^3J_{H^NH^\alpha}$ and $^3J_{H^NC'_i}$ **b** the four proton-involving couplings **c** all six ϕ related couplings. The following subsets of five and four coupling constants are expected to fully avoid ambiguities in the dihedral-angle angle determination in the regime of rigid local geometry: **d** all six *J* except $^3J_{H^NC^\beta}$; **e** $^3J_{H^NH^\alpha}$, $^3J_{H^NC'_i}$, $^3J_{C'_{i-1}H^\alpha}$ and $^3J_{C'_{i-1}C'_i}$; **f** $^3J_{H^NC'_i}$, $^3J_{H^NC^\beta}$ $^3J_{C'_{i-1}H^\alpha}$ and $^3J_{C'_{i-1}C'_i}$. *White*, *grey* and *black* regions represent (ϕ, ϕ) pairs, distinguishable by none, a single or two couplings, respectively. For further details see Fig. 4

in Fig. 2: two narrow and two broader white regions with dihedral angles, that all have degenerate coupling constants within the given confidence interval. In the case where motional averaging is absent, a unique ϕ dihedral-angle is determined for any grey off-diagonal region in the map. Trivially, white diagonal stretches must remain. Thus ambiguity maps reveal both the limits of the pure *J* coupling analysis and the extent of independent information in a set of different couplings.

The key to resolve the degeneracy inherent to each of the contributing coupling constants lies in an additive combination. As an example Fig. 5 a presents the ambiguity plot for the simultaneous use of $^3J_{H^NH^\alpha}$ and $^3J_{H^NC'}$. (ϕ, ϕ) dihedral angle pairs, that can be discriminated by none (white), a single (grey) or both (black) of these coupling constants are indicated. Although some ambiguity is removed, three white off-diagonal spots remain, thus necessitating the use of additional coupling information. Unfortunately, two of these off-diagonal regions at $\phi \approx +80°$ and $\phi \approx +170°$ are degenerate with ϕ angles around –60° which are typical of α-helices. It is concluded that these two coupling constants do not contain sufficient information for a reliable determination of the ϕ dihedral angle in an α-helical situation.

The uniqueness in the dihedral-angle determination can be improved by combining, for example, all four proton-involving couplings $^3J_{H^NH^\alpha}$, $^3J_{H^NC'}$, $^3J_{H^NC^\beta}$, and $^3J_{C'_{i-1}H^\alpha}$, as shown in Fig. 5 b. Still, ambiguity persists for the regions around $\phi \approx -60°$ and $\phi \approx +170°$. Inclusion of $^3J_{C'_{i-1}C'_i}$ and $^3J_{C'_{i-1}C^\beta}$ coupling information, i. e. the combined use of all 6 ϕ related couplings completely avoids any ambiguity as depicted in Fig. 5 c. Subsets of couplings ambiguity are shown in Fig. 5 d for a combination of five and in Fig. 5 e, f for combinations of four couplings, respectively.

In order to quantify the ambiguity areas, the percentage of (ϕ, ϕ) dihedral angle pairs with an arbitrarily chosen minimum difference of 25°, which can be distinguished by either none, one, two, or more than two coupling constants, has been calculated. Table 4 lists the most important results. Taken as an example, 2.5% of the (ϕ, ϕ) pairs differing by more than 25° cannot be discriminated using $^3J_{H^NH^\alpha}$ and $^3J_{H^NC'}$ (Fig. 5 b) or either combination of three coupling constants. Interestingly, best acceptable results are expected from $^3J_{H^NH^\alpha}$ and $^3J_{H^NC'}$ combined with either $^3J_{C'_{i-1}H^\alpha}$ or $^3J_{C'_{i-1}C'_i}$.

When combining four couplings to resolve the degeneracy of the Karplus relation, best results can be anticipated for $^3J_{H^NC'}$, $^3J_{C'_{i-1}H^\alpha}$, and $^3J_{C'i-1C\hat{i}}$ combined with either $^3J_{H^NC^\beta}$ (Fig. 5 e) or $^3J_{H^NH^\alpha}$ (Fig. 5 f). These combinations allow a complete solution of the ambiguity and thus are suitable for a ϕ torsion angle analysis. The remaining regions of ambiguity are due to a broad diagonal with $25° < \Delta\phi < 30°$.

Indeed, combining the four proton-involved couplings with $^3J_{C'_{i-1}C'_i}$ leads to a complete solution of the ambiguity (Fig. 5 d), while sets of the ϕ related couplings disregarding either $^3J_{C'_{i-1}H^\alpha}$ or $^3J_{C'_{i-1}C'_i}$ are unfavourable, as they still invoke ambiguity problems (Table 4).

Table 4 Quantitative description of the ambiguity diagrams [a]

$^3J_{H^NH^\alpha}$	$^3J_{H^NC'}$	$^3J_{H^NC^\beta}$	$^3J_{C'_{i-1}H^\alpha}$	$^3J_{C_{i-1}C'_i}$	$^3J_{C'_{i-1}C^\beta}$	Numbers of couplings to distinguish ϕ/ϕ pairs: 0	1	2	≥3	Comments	Figure
6	–	–	–	–	–	17.1	82.9	–	–	$^3J_{H^NH^\alpha}$ exclusively	4a
6	b	–	–	–	–	2.5	38.5	59.0	–	$^3J_{H^NH^\alpha}$ and $^3J_{H^NC'}$	5a
6	b	–	V	–	–	0.9	14.8	38.5	45.9	best with three couplings	
6	b	–	–	*β*	–	0.9	23.4	50.3	25.4	best with three couplings	
–	b	iii	V	*β*	–	0.0	11.4	32.2	56.4		5e
6	b	–	V	*β*	–	0.0	8.7	28.1	63.2	best with four couplings	5f
6	–	iii	V	*β*	–	0.1	9.0	29.3	61.6	best with four couplings	5f
6	b	iii	V	–	–	0.7	2.6	22.7	74.0	proton-related only couplings	5b
6	b	iii	–	–	*D*	1.4	3.6	32.0	63.0	worst with four couplings	
–	–	iii	V	*β*	*D*	4.0	11.3	36.4	48.4	worst with four couplings	
6	b	–	V	*β*	*D*	0.0	1.4	19.8	78.8	best with five couplings	5d
6	b	iii	V	*β*	–	0.0	1.5	14.5	84.0	best with five couplings	5d
–	b	iii	V	*β*	D	0.0	5.8	20.7	73.5	best with five couplings	5d
6	b	iii	V	–	*D*	0.3	2.1	11.1	86.5	worst with five couplings	
6	b	iii	–	*β*	*D*	0.5	2.1	19.4	78.1	worst with five couplings	
6	b	iii	V	*β*	*D*	0.0	0.9	6.9	92.3	all six couplings	5c

[a] The combination of the employed couplings indexed with the code from Table 1 is followed by the percentage of the possible ϕ/ϕ dihedral angle pairs, that can be discriminated by none, one, two or more than two couplings

Table 5 Quantitative results for the back-calculated coupling constants of selected residues [a]

Residue		Coupling constants [Hz]						ϕ Torsion [deg]	Signif. [%]
		$^3J_{H^NH^\alpha}$	$^3J_{H^NC'}$	$^3J_{H^NC^\beta}$	$^3J_{C'_{i-1}H^\alpha}$	$^3J_{C'_{i-1}C'}$	$^3J_{C'_{i-1}C^\beta}$		
Ile 65	exp.	6.80	1.02	2.12	2.54	0.58	2.82		
	rigid	6.82	0.31	2.12	1.88	0.52	2.91	–81.8	97.9
	Gauss	6.73	0.70	1.83	1.93	0.70	2.63	–83.5±20.9	99.4
Leu 112	exp.	3.54	1.43	2.33	0.68	1.01	3.59		
	rigid	3.73	1.83	2.44	1.07	0.53	3.27	–57.5	98.7
	Gauss	3.08	1.91	2.84	1.96	2.20	1.54	153.4±29.9	32.1
Glu 118	exp.	7.25	0.18	1.33	2.93	0.30	1.90		
	rigid	7.86	0.06	1.77	2.22	0.63	2.57	–90.7	95.8
	Gauss	7.66	0.46	1.54	2.20	0.83	2.31	–93.9±20.4	98.7
Asp 76	exp.	3.74	1.48	2.46	1.38	0.40	3.24		
	rigid	3.94	1.69	2.44	1.11	0.52	3.28	–59.3	100
	Gauss	3.94	1.69	2.44	1.11	0.52	3.28	–59.3±0	99.6

[a] The values for the experimental coupling constants are compared to values derived from the fit procedure, when assuming either a single rigid conformation or a Gaussian distribution. The model with the highest statistical significance is selected for further analysis

ϕ dihedral angle analysis in flavodoxin

Having identified the necessary couplings and the optimal combination of Karplus parameter sets, a comprehensive ϕ dihedral angle analysis has been performed for flavodoxin based solely on quantitative coupling constants. Apart from the residues Thr 15, Leu 55, and Asp 63, altogether 123 out of the 126 non-glycine and non-proline residues were considered in the analysis. Figure 6 shows the limits of a pure *J* coupling analysis based on only three coupling constants. Two situations are presented, where three couplings contain sufficient (Fig. 6A) and insufficient (Fig. 6B) information for a unique determination of the corresponding ϕ dihedral angle.

When combining all four proton-involved couplings, for most of the residues the degenerate solutions were qualitatively excluded and a unique ϕ dihedral angle was derived. As already predicted by the ambiguity map shown in Fig. 5b, the determination of ϕ angles typical of α-helix conformations with $-55° < \phi < -35°$ is still difficult. An example is shown in Fig. 6C. The consideration of all six available coupling constants allows the unique determination of the corresponding ϕ dihedral angle (Fig. 6D).

Three different models of angular motion about the N-C$^\alpha$ bond have also been taken into account (Schmidt 1997): a rigid conformation, a Gaussian distribution of dihedral angles, and an equilibrium between two distinct dihedral angles.

For 90 out of 123 investigated residues, the rigid-torsion model conforms with the experimental coupling constants. Out of these, 82 torsions agreed within ±10° with the values found in the the crystal structure. The larg-

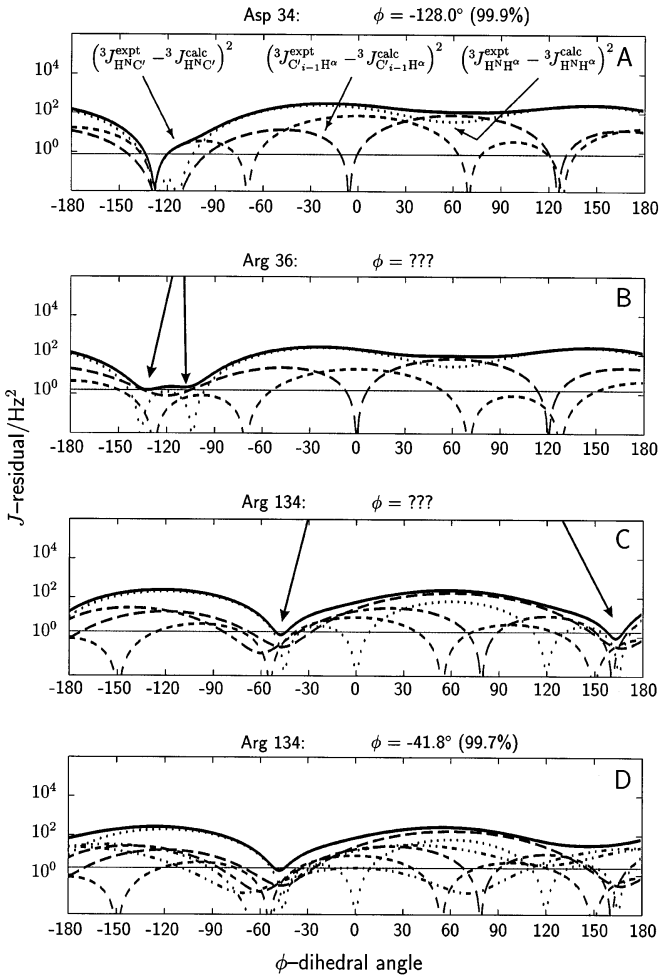

Fig. 6 A–D Examples for the pure ^3J coupling based dihedral-angle analysis. Error profiles for the individual coupling types are shown as *broken lines*. The summed error is represented by a *thick solid line*, where minima indicate ϕ dihedral angles in closest agreement with the experimental data. Obviously, $^3J_{H^NH^\alpha}$, $^3J_{H^NC'_i}$, and $^3J_{C_{i-1}H^\alpha}$ values are sufficient to determine a unique ϕ conformation for Asp 34 (panel **A**), while for Arg 36 a broad minimum is detected (panel **B**), requiring additional coupling data. A ϕ angle analysis based on all four proton-involved couplings fails for residues with $-55° < \phi < -35°$ due to an alternative solution of $+160° < \phi < \pm 180°$ (panel **C**). As shown for Arg 134, consideration of all six ϕ related couplings rules out the false positive ϕ values (panel **D**)

est discrepancy was detected at Leu 78, for which ϕ values in the solid and solution state differ by approximately 24°.

For 32 residues the agreement between experimental and calculated coupling constants improved when assuming a Gaussian distribution of ϕ-dihedral angles with widths from ±3° to ±21° around one distinct angle. The Gaussian distributions were concentrated at residues located in loops connecting secondary-structure elements and in the C-terminal tail.

Only a single case (Glu 42) emerged for which the motional model of an equilibrium of two conformations with an almost equal population describes the experimental data best. A two-site jump between the two ϕ dihedral angles –127.0° and –94.1° also confirms the observation of two separate conformations in an ensemble of structures based solely on NOE data (to be published elsewhere).

Table 2 summarizes the results with the highest significance for each residue and provides the values from the X-ray structure for comparison. In Table 5 the fit results of four selected residues are compiled. A graphical representation of the results is presented in Fig. 7.

Comparison with X-ray data

Despite the fact that parameter averaging is affected by different processes in solution and in the crystal, it is instructive to compare the motional models as suggested by the *J*-coupling analysis with isotropic B factors for the C^α- and N-backbone atoms as obtained in X-ray spectroscopy. Figure 7 shows that angular Gaussian distributions, whenever found for a particular residue in flavodoxin, correlate strikingly with elevated B values. Interestingly, the largest B factors, disregarding the C-terminal atoms, are assigned to residue Glu 42 for which the *J*-coupling analysis revealed a two-site conformational exchange. The observation of two distinct conformations in a distance-geometry ensemble calculation (unpublished) support the unusual geometry in the region of Glu 42. It is therefore concluded that two conformations superimposed in the X-ray structure refinement are likely to improve the fit of the electron-density map (Karimi-Nejad et al. 1994). However, crystal-packing effects are made responsible for a comparatively rigid loop region at residues Asp 28 and Ala 29 which both exhibit extensive mobility according to the NMR analysis.

Of particular interest are conformations of residues expected to interact with the FMN cofactor in the binding site. Asp 62 adopts an energetically unfavourable positive ϕ value according to both X-ray and NMR analysis. Detailed *J*-coupling analysis revealed a broad ±19.1° distribution about $\langle\phi\rangle = +67.9°$ in the solution state. The adjacent residue Gly 61, which could not be included in the present *J*-coupling analysis, is known to undergo a major conformational change upon reduction of flavodoxin leading to formation of a new hydrogen bond with the FMN (Watt et al. 1991). Obviously, the concerted conformational equilibrium and dynamic properties of the residues Gly 61 and Asp 62 delicately modulate the electrochemical properties of the one-electron reduced semiquinone form of FMN bound to the apoprotein (Mayhew and Tollins 1992).

Conclusions

Distinct Karplus parametrizations for ϕ related couplings found in the literature have been compared. The core of *Desulfovibrio vulgaris* flavodoxin with the secondary structure-elements was used as a reference to identify the

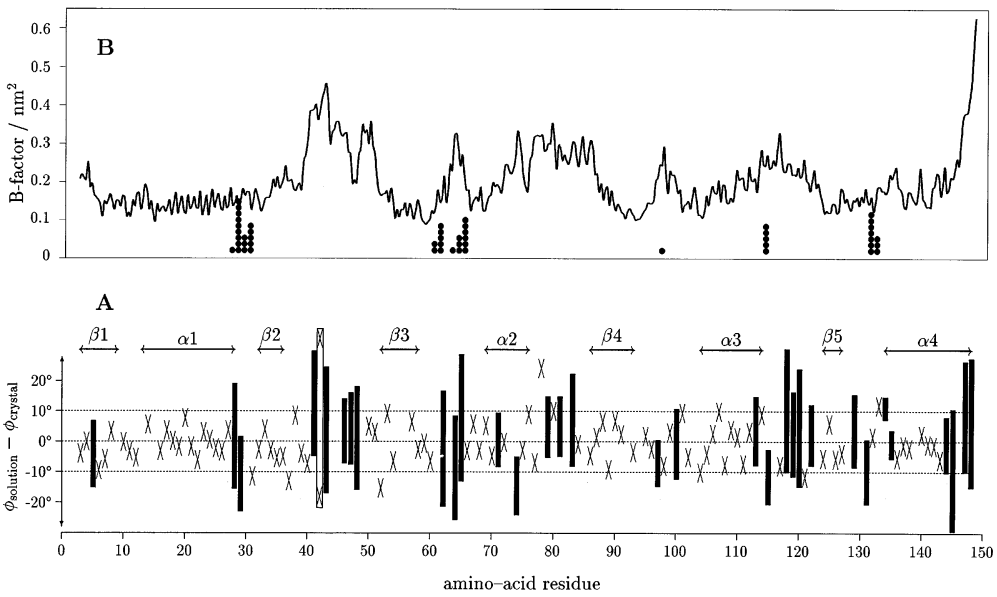

Fig. 7 A, B Overview of the ϕ-torsion analysis for flavodoxin. **A**: Residues found to adopt a rigid conformation are indicated by crosses vertically shifted to respect the difference between ϕ dihedral angle conformations in aqueous and crystalline environment. *Vertical bars* indicate the width $\pm 2\sigma$ of a Gaussian distribution for the mobile residues. The range of the secondary structure elements is marked by *arrows*. **B** Crystallographic B-factors of the C′-, C^{α}- and N-backbone atoms from the X-ray structure. The number of intermolecular contacts shorter than 450 pm involving backbone atoms is shown by *black dots* at the residue number

influence of different parameter sets on the dihedral-angle analysis. The best correlation with the values of a reference X-ray structure has been achieved, when the parameters indicated with an asterisk in Table 1 were used in the evaluation.

The new introduced ambiguity map allows one to explore the limits of a reliable determination of dihedral angles with *J* coupling constants. A complete analysis of ϕ angles requires quantitative values for at least four different couplings: $^3J_{H^N C'}$, $^3J_{C'_{i-1} H^{\alpha}}$, and $^3J_{C'_{i-1} C'_i}$ together with either $^3J_{H^N H^{\alpha}}$ or $^3J_{H^N C^{\beta}}$. The concerted use of all six couplings provides both a solution of the Karplus degeneracy and a large amount of redundant information. Even distributions of angular adjustments can be considered in the simulation of experimental coupling constants. Most of the residues exhibit rigid conformations, while in loop regions Gaussian distributions of angles or equilibria of two conformations are in best accordance to the experimental data.

In a protein-structure calculation the derived ϕ angles have been considered as angular constraints with margins of ±10° centered at the dihedral angle value derived. When a Gaussian distribution of dihedral angle conformations was found to be optimal for fitting the data, the constraint width was set to $\pm 2\sigma$. The precision of the structure ensemble derived has been improved considerably (to be published elsewhere).

The precise function of flavodoxin in the sulfate-reduction pathway is still unknown. Presumably the special geometry of residues in the loop containing Glu 42 and in the FMN-binding region (Asp 62) influence the biochemical activity of flavodoxin. In protein structures determined solely on the basis of NOE data these regions are poorly defined, whereas the dispersed conformations of the ϕ torsion angles can be described by the quantitative *J* coupling analysis of the six ϕ dihedral angle related coupling types.

Acknowledgements We thank Dr. M. Knauf and Prof. S. Mayhew for their help in preparing recombinant isotope enriched flavodoxin. The help of Roland Weiss in the determination of the $^3J_{H^N H^{\alpha}}$ coupling constants is acknowledged. The research was supported by grants from the Deutsche Forschungsgemeinschaft (Ru 145/11-2). Thanks are due to Dr. Martin Walsh from the EMBL in Hamburg for making available the 170-pm X-ray structure of flavodoxin prior to publication.

References

Archer SJ, Ikura M, Torchia DA, Bax A (1991) An alternative 3D NMR technique for correlating backbone ^{15}N with side chain Hβ resonances in larger proteins. J Magn Reson 95: 636–641

Biamonti C, Rios CB, Lyons BA, Montelione GT (1994) Multidimensional NMR experiments and analysis techniques for determining homo- and heteronuclear scalar coupling constants in proteins and nucleic acids. Adv Biophys Chem 4: 51–120

Billeter M, Neri D, Otting G, Qian YQ, Wüthrich K (1992) Precise vicinal coupling constants $^3J_{H^N H^{\alpha}}$ from nonlinear fits of *J*-modulated [^{15}H, ^1H]-COSY-experiments. J Biomol NMR 2: 257–274

Bystrov VF, Ivanov VT, Portnova SL, Balashova TA, Ouchinnikov YA (1973) Refinement of the angular dependence of the peptide vicinal NH-$C^{\alpha}H$ coupling constant. Tetrahedron 29: 873–877

Bystrov VF, Gavrilov YD, Solkan VN (1975) Stereochemical dependence of the vicinal $^{13}C'$-NC^{α}-^1H and ^1H-$C^{\alpha}C'$-^{15}N proton-heteroatom coupling constants in the NMR spectra of Peptides. Comparison of experimental and theoretical data. J Magn Reson 19: 123–129

Bystrov VF (1976) Spin-spin coupling and the conformational states of peptide systems. Prog NMR Spectrosc 10: 41–81

Case DA, Dyson HJ, Wright P (1994) Use of chemical shifts and coupling constants in nuclear magnetic resonance structural studies on peptides and proteins. Meth Enzymol 239: 392–416

Chothia C (1984) Principles that determine the structures of proteins. Annu Rev Biochem 53: 537–572

Clifford AA (1973) A handbook of multivariate error analysis. London, UK, Applied Science Publishers Ltd

Curley GP, Voordouw G (1988) Cloning and sequencing of the gene encoding flavodoxin from *Desulfovibrio vulgaris* (Hildenborough). FEMS Microbiol Lett 49: 295–299

Curley GP, Carr MC, Mayhew SG, Voordouw G (1991) Redox and flavin-binding properties of recombinant flavodoxin from *Desulfovibrio vulgaris* (Hildenborough). Eur J Biochem 202: 1091–1100

DeMarco A, Llinás M, Wüthrich K (1978) Analysis of the ^{1}H-NMR spectra of ferrichrome peptides. I. The non-amide protons. Biopolymers 17: 637–650

Dubourdieu M, Fox JL (1977) Amino acid sequence of *Desulfovibrio vulgaris* flavodoxin. J Biol Chem 252: 1453–1459

Eberstadt M, Gemmecker G, Mierke DM, Kessler H (1995) Skalare Kopplungen – ihre Analyse und ihre Verwendung zur Strukturaufklärung. Angew Chem 107: 1813–1838; Angew Chem Int Ed 34: 1671–1695

Edison AS, Markley JL, Weinhold F (1994) Calculations of one-, two- and three-bond nuclear spin-spin couplings in a model peptide and correlations with experimental data. J Biomol NMR 4: 519–542

Emseley L, Bodenhausen G (1990) Gaussian pulse cascades: New analytical functions for rectangular selective inversion and in-phase excitation in NMR. Chem Phys Lett 165: 469–476

Ghisla S, Massey V (1989) Mechanisms of flavoprotein catalyzed reactions. Eur J Biochem 181: 1–17

Hoch JC, Dobson CM, Karplus M (1985) Vicinal coupling constants and protein dynamics. Biochemistry 24: 3831–3841

Hu JS, Bax A (1996a) Measurement of three-bond ^{13}C-^{13}C *J* couplings between carbonyl and carbonyl/carboxyl carbons in isotopically enriched proteins. J Am Chem Soc 118: 8170–8171

Hu JS, Bax A (1996b) XVIIth International Conference on Magnetic Resonance in Biological Systems (August 18–23, 1996) Keystone, USA, poster TP21

IUPAC-IUB Commission on Biochemical Nomenclature (1970) Abbreviations and symbols for the description of the conformation of polypeptide chains. Biochemistry 9: 3471–3479

Jardetzky O (1980) On the nature of molecular conformations inferred from high-resolution NMR. Biochem Biophys Acta 621: 227–232

Kao LF, Barfield M (1985) Conformational dependencies of vicinal ^{13}C(O)-N-C$^{\alpha}$-^{13}C and ^{13}C(O)-N-C$^{\alpha}$-^{1}H coupling constants in compounds which model the peptide backbone. J Am Chem Soc 107: 2323–2330

Karimi-Nejad Y, Schmidt JM, Rüterjans H, Schwalbe H, Griesinger C (1994) Conformation of valine side chains in ribonuclease T1 determined by NMR studies of homonuclear and heteronuclear ^{3}J coupling constants. Biochemistry 33: 5481–5492

Karplus M (1959) Contact electron-spin coupling of nuclear magnetic resonance. J Chem Phys 30: 11–15

Karplus M (1963) Vicinal proton coupling in nuclear magnetic resonance. J Am Chem Soc 85: 2870–2871

Kay LE, Keifer P, Saarinen T (1992) Pure absorption gradient enhanced heteronuclear single quantum correlation spectroscopy with improved sensitivity. J Am Chem Soc114: 10663–10665

Knauf MA, Löhr F, Curley GP, O'Farrell P, Mayhew SG, Müller F, Rüterjans H (1993) Homonuclear and heteronuclear NMR studies of oxidized *Desulfovibrio vulgaris* flavodoxin. Eur J Biochem 213: 167–184

Knauf MA, Löhr F, Blümel M, Mayhew SG, Rüterjans H (1996) NMR investigation of the solution conformation of oxidized flavodoxin from *Desulfovibrio vulgaris*. Determination of the tertiary structure and detection of protein-bound water-molecules. Eur J Biochem 238: 423–434

Kuboniwa H, Grzesiek S, Delaglio F, Bax A (1994) Measurement of H^{N},H$^{\alpha}$ *J*-couplings in calcium-free calmodulin using new 2D and 3D water-flip-back methods. J Biomol NMR 4: 871–878

Laskowski RA, Moos DS (1993) Main-chain bond lengths and bond angles in protein structures. J Mol Biol 231: 1049–1067

Löhr F, Rüterjans H (1995) (H)NCAHA and (H)CANNH experiments for the determination of vicinal coupling constants related to the ϕ-torsion angle. J Biomol NMR 5: 25–36

Löhr F, Blümel M, Schmidt JM, Rüterjans H (1997) Application of H(N)CA,CO-E COSY experiments for calibrating the ϕ-angular dependences of vicinal couplings $^{3}J_{C'_{i-1}H^{\alpha}}$, $^{3}J_{C'_{i-1}C'_{i}}$, and $^{3}J_{C'_{i-1}C^{\beta}}$ in proteins. J Biomol NMR 10: 107–118

Ludvigsen S, Andersen KV, Poulsen FM (1991) Accurate measurements of coupling constants from two-dimensional nuclear magnetic resonance spectra of proteins and determination of ϕ-angles. J Mol Biol 217: 731–736

Madsen JC, Sørensen OW, Sørensen P, Poulsen FM (1993) Improved pulse sequences for measuring coupling constants in ^{13}C, ^{15}N-labeled proteins. J Biomol NMR 3: 239–244

Mayhew SG, Tollin G (1992) In: Müller F (ed) Chemistry and Biochemistry of flavoenzymes. Structure and redox properties of *Clostridial* flavodoxin. Boca Raton, USA, CRC Press 3rd ed, vol 3, pp 389–426

Mierke DF, Kessler H (1992) Combined use of homo- and heteronuclear coupling constants as restraints in molecular dynamics simulations. Biopolymers 32: 1277–1282

Nelder JA, Mead R (1965) A simplex method for function minimization. Computer Journal 7: 308–313

Neri D, Otting G, Wüthrich K (1990) New nuclear magnetic resonance experiments for measurements of the vicinal coupling constants $^{3}J_{\mathrm{HN}\alpha}$ in proteins. J Am Chem Soc 112: 3663–3665

Pardi A, Billeter M, Wüthrich K (1984) Calibration of the angular dependence of the amide proton-C$^{\alpha}$ Proton coupling constants, $^{3}J_{HN\alpha}$, in a globular protein. J Mol Biol 180: 741–751

Peng JW, Wagner G (1992) Mapping of the spectral density functions using heteronuclear relaxation experiments. J Magn Reson 98: 308–332

Piotto M, Sandek U, Sklenář U (1992) Gradient-tailored excitation for single-quantum NMR spectroscopy of aqueous solutions. J Biomol NMR 2: 661–665

Roberts GCK (ed) (1993) NMR of Macromolecules: A Practical Approach. Oxford, UK, Oxford University Press

Schleucher J, Schwendinger M, Sattler M, Schmidt P, Schedletzky O, Glaser SJ, Sørensen OW, Griesinger C (1994) A general enhancement scheme in heteronuclear multi-dimensional NMR employing pulsed field gradients. J Biomol NMR 4: 301–306

Schmidt JM, Ernst RR, Aimoto S, Kainosho M (1995) Determination of heteronuclear three-bond coupling constants in peptides by a simple heteronuclear relayed E COSY experiment. J Biomol NMR 6: 95–105

Schmidt JM, Löhr F, Rüterjans H (1996) Heteronuclear relayed E COSY applied to the determination of accurate ^{3}J(H^{N},C′) and ^{3}J(H$^{\beta}$, C′) coupling constants in *Desulfovibrio vulgaris* flavodoxin. J Biomol NMR 7: 142–152

Schmidt JM (1997) Conformational equilibria in polypeptides II. J Magn Reson 124: 310–322

Schwalbe H, Rexroth A, Eggenberger U, Geppert T, Griesinger C (1993) Measurement of C′,C coupling constants in ^{13}C labeled proteins: A new method for the stereospecific assignment of γ-methyl-groups in valine residues. J Am Chem Soc 115: 7878–7879

Seip S, Balbach J, Kessler H (1994) Determination of backbone conformation of isotopically enriched proteins based on coupling constants. J Magn Reson B 104: 172–179

Sokal RR, Rohlf FJ (1981) Biometry – Statistical Tables. Freeman WH, New York, USA, 2nd ed

Solkan VN, Bystrov VF (1974) Bull Acad Sci USSR (Div Chem Sci) 23: 1232

Vuister GV, Bax A (1993) Quantitative *J* correlation: a new approach for measuring homonuclear three-bond J(H^{N}H$^{\alpha}$) coupling constants in ^{15}N-enriched proteins. J Am Chem Soc 115: 7772–7777

Waits DG (1994) Parameter estimates from nonlinear models. Meth Enzymol 240: 23–36

Wang AC, Bax A (1996) Determination of the backbone dihedral angles ϕ in human ubiquitin from reparametrized empirical Karplus equations. J Am Chem Soc 118: 2483–2494

Watt W, Tulinsky A, Swenson RP, Watenpaugh KD (1991) Comparison of the crystal structures of a flavodoxin in its three oxidation states at cryogenic temperatures. J Mol Biol 218: 195–208